Physical Chemistry

Multidimensional tunneling dynamics of proton transfer in malonaldehyde molecule and its isotopomers

V. A. Benderskii,[a] E. V. Vetoshkin,[a] I. S. Irgibaeva,[a] and H.-P. Trommsdorff[b]*

[a]Institute of Problems of Chemical Physics, Russian Academy of Sciences, 142432 Chernogolovka, Moscow Region, Russian Federation. Fax: +7 (096) 576 4009. E-mail: bend@b5570.home.chg.ru
[b]Laboratoire de Spectrometrie Physique, Université J. Fourier de Grenoble, France. Fax: (+33) 4765 14544. E-mail: hans-peter.trommsdorff@ujf-grenoble.fr

The twenty-one-dimensional Hamiltonian of malonaldehyde molecule and a number of its isotopomers (H/D, $^{13}C/^{12}C$) was reconstructed in the low-energy region (<3000 cm^{-1}). Parameters of the Hamiltonian were obtained from quantum-chemical calculations of the energies, equilibrium geometries, and eigenvectors and eigenfrequencies of normal vibrations at the stationary points corresponding to the ground state and transition state. Despite substantial variation of the barrier height calculated using different quantum-chemical methods (from 2.8 to 10.3 kcal mol^{-1}), the corresponding potential energy surfaces can be matched with high accuracy by scaling only one parameter (the semiclassical parameter γ, which defines the scales of potential, energy, and action). Scaling invariance allows optimization of the Hamiltonian in such a way that the calculated ground-state tunneling splitting coincides with the experimental value. The corresponding potential barrier height is estimated at 4.34±0.4 kcal mol^{-1}. The quantum dynamics problem was solved using the perturbative instanton approach without reducing the number of degrees of freedom. The role of all transverse vibrations in proton tunneling is characterized. Vibration-tunneling spectrum is calculated for the ground state and low-lying excited states and mode-specific isotope effects are predicted.

Key words: multidimensional tunneling, tunneling splittings, malonaldhyde, proton transfer, vibration-tunneling spectra.

Malonaldehyde (MA, Fig. 1) is one of the simplest molecules with intramolecular hydrogen transfer in two tautomers separated by a potential barrier. The experimental ground-state tunneling splitting, ΔE_0 = 647046.208±0.019 MHz,[1,2] is two orders of magnitude larger than that predicted from the penetrability factor of one-dimensional (1D) barrier. The increase in the splitting is due to significant changes in the equilibrium geometry along the tunneling path, *i.e.*, to displacements along the small-amplitude coordinates which decrease the width of the potential barrier, thus stimulating tunneling. In the MA molecule, the tunneling coor-

Published in Russian in *Izvestiya Akademii Nauk. Seriya Khimicheskaya,* No. 7, pp. 1096—1105, July, 2001.

1066-5285/01/5007-1148 $25.00

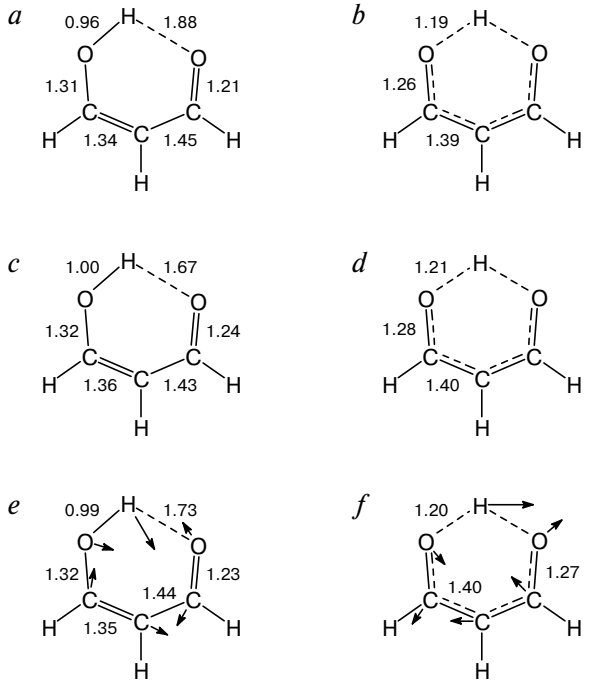

Fig. 1. Ground-state (*a*, *c*, *e*) and transition-state (*b*, *d*, *f*) geometries of malonaldehyde molecule (bond lengths/Å) calculated by the HF/6-31G** (*a*, *b*) and B3LYP/6-31+G(2d,p) (*c*, *d*) methods and using the optimized Hamiltonian (*e*, *f*). The eigenvectors of the ν_8 vibration corresponding to the tunneling coordinate X in the transition state are shown.

dinate is strongly coupled with such vibrations. This makes the situation convenient for multidimensional tunneling studies.

Recently, we have developed the perturbative instanton approach (PIA).[3—12] In this work, the PIA was used to describe the multidimensional tunneling dynamics of proton transfer in MA. We will show that this approach allows refinement of the results obtained in quantum-chemical calculations of the potential energy surface (PES) of the MA molecule, quantitative characterization of the role of all vibrations in the multidimensional tunneling, and calculations of vibration-tunneling spectra.

The instanton formalism[13,14] (see also reviews[15,16]) has previously been employed in solving model problems of chemical dynamics.[17—20] It was also used in studies of real nonrigid molecules.[21—25] The corresponding $(3N - 6)$-dimensional PES were reconstructed using the results of quantum-chemical calculations of changes in the equilibrium geometries and frequencies of normal vibrations in the transition state compared to the ground-state parameters. The role of particular vibrations in multidimensional tunneling was established.[21—25] However, there is a need to refine the results obtained in these studies. It stems from the fact that the authors of the above-mentioned communications used a simplified version of the instanton approach, in which (i) the extreme tunneling trajectory (ETT) is replaced by the minimum energy path (MEP) and (ii) the totally symmetric (squeezed) potential couplings and all kinematic couplings are ignored. This precluded optimization of the PES and calculations of tunneling splittings in excited vibrational states.

The PIA [3—12] does not require the above-mentioned simplifications. Earlier,[3] we have reported the results of preliminary analysis of proton transfer in MA and emphasized that replacement of the ETT by the MEP [21] leads to substantial overestimation of the effect of transverse vibrations. Yet another reason for the revision of published results[21] is associated with overestimation of the adiabatic potential barrier height (10.3 kcal mol^{-1}). Modern quantum-chemical estimates[26,27] of this parameter are much lower (from 3.9 to 4.2 kcal mol^{-1}).

Reconstruction of the vibrational Hamiltonian

The MA molecule has a planar geometry. In the ground and transition states, it belongs to the C_s and C_{2v} point groups of symmetry, respectively. The isodynamic group $C_2 \otimes C_s$ is isomorphic to the transition-state point group. The vibrational Hamiltonian was reconstructed in the reactive coordinates (see Refs. 5, 7, 11). The large-amplitude coordinate X belongs to the A′ and B_2 irreducible representations in the C_s and C_{2v} point groups, respectively. This coordinate is coupled with twenty small-amplitude transverse vibrations $\{Y_k\}$.

The type of coupling is determined as follows. If two coordinates, X and Y_k, belong to the same irreducible representations in both point groups of symmetry, the XY_k-coupling is called linear (L). If these coordinates belong to the same irreducible representation only in the C_s group, the XY_k-coupling is called gated (G). It a pair of coordinates does not belong to the A′ and B_2 irreducible representations, the coupling is called totally symmetric, or squeezed (Sq). Both L-coupled and G-coupled vibrations can also be Sq-coupled.

Thus, the set of transverse modes for the MA molecule includes six L-coupled, eight G-coupled, and six Sq-coupled vibrations. The potential energy corresponding to the three types of coupling can be expanded in powers of the reactive coordinates $(X,\{Y_k\})$. Neglecting X-independent anharmonicity of transverse vibrations leads to the following expression for the PES[7—9]

$$V(X,\{Y_k\}) = V_0(X) + \sum_{k\subset \mathrm{L}} C_k X(C_k X/2\omega_k^2 - Y_k) + \\ + \sum_{k\subset \mathrm{G}} C_k (1 - X^2) Y_k + \sum_{k\subset \mathrm{L,G,Sq}} 0.5\omega_k^2(1 + \alpha_{kk} X^2/\omega_k^2) Y_k^2 + \\ + \sum_{k,k'\subset \mathrm{L}} \alpha_{kk'} X^2 (Y_k - C_k X/\omega_k^2)(Y_{k'} - C_{k'} X/\omega_{k'}^2) + \\ + \sum_{k\subset \mathrm{L},k'\subset \mathrm{G}} \alpha_{kk'} X(Y_k - C_k X/\omega_k^2) Y_{k'} + \sum_{k,k'\subset \mathrm{G,Sq}} \alpha_{kk'} X^2 Y_k Y_{k'}, \quad (1)$$

where ω_k are the dimensionless frequencies (see the text below), C_k are the L- and G-coupling constants, and α_{kk} are the Sq-coupling constants. In contrast to the conventional approximation of noninteracting transverse

vibrations, the PES given by expression (1) includes the X-dependent $Y_kY_{k'}$-interactions characterized by the $\alpha_{kk'}$ coupling constants. These interactions are responsible for the mixing of transition-state normal modes along the MEP. The 1D double-well potential used in this work has a more general form than previously[3,4,21]:

$$V_0(X) = 0.5 \sum_{m=2,3,4} V_m (1 - X^2)^m. \qquad (2)$$

We introduce the quasiclassical parameter γ as the square of the ratio of the tunneling distance, a_0, to the amplitude of zero-point vibrations at the minimum of the 1D potential:

$$\gamma = m_0\Omega_0 a_0^2/(2\hbar), \qquad (3)$$

where m_0 and Ω_0 are the mass and eigenfrequency of the X-vibration at the minimum of the 1D potential.

Expression (1) for the PES is written in dimensionless coordinates (here, the action, energy, and potential energy are measured in units of γ, $\hbar\Omega_0$, and $\gamma\hbar\Omega_0$, respectively). The dimensionless transverse frequencies ω_k are defined as the ratios of the frequencies to Ω_0. The PES defined by Eqs. (1) and (2) is characterized by 143 parameters. These are 3 parameters of the 1D potential (m = 2, 3, 4), 14 L- and G-coupling constants (C_k), 20 Sq-coupling constants (α_{kk}), and 106 YY'-coupling constants ($\alpha_{kk'}$). The kinematic matrix with X-dependent coefficients is uniquely determined by the type of potential couplings[6] and contains 141 constants.

Multidimensional tunneling is characterized by the spectral densities of the L- and G-vibrations, defined as follows[3]

$$\rho_L = \sum_{k\subset L} (C_k/\omega_k^2)^2, \qquad \rho_G = \sum_{k\subset G} (C_k/\omega_k)^2. \qquad (4)$$

The ρ_G value characterizes a decrease in the adiabatic barrier height as compared to the 1D barrier height

$$V_{ad} = V_0^{\#}(1 - \rho_G), \qquad (5)$$

whereas ρ_L determines the lengthening of the MEP as compared to the 1D path. The action along the ETT between the 1D potential minima includes the contributions of both L- and G-vibrations which increase (L) or decrease (G) the 1D action (W^*), thus assisting or suppressing tunneling, respectively:

$$W^* = W_0^* + \tilde{\rho}_L - \tilde{\rho}_G,$$
$$\tilde{\rho}_L = \sum_{k\subset L} (C_k/\omega_k^2)^2 F^L(\omega_k),$$
$$\tilde{\rho}_G = \sum_{k\subset G} (C_k/\omega_k)^2 F^G(\omega_k). \qquad (6)$$

Here, $\tilde{\rho}_L$ and $\tilde{\rho}_G$ are the modified spectral densities. The possibility of introduction of these parameters is due to universal character of the functions $F(\omega_k)$ [3] (see also Ref. 11), which depend on the shape of the 1D potential. As the frequency increases, the functions $F(\omega_k)$ vary from $F(0) = 0$ to $F(\infty) = 1$ in such a manner that the contributions of transverse vibrations to the action in the adiabatic limit ($\omega\to\infty$) are equal to the spectral densities defined by relationships (4). As ω_k decrease, these contributions also decrease and become zero in the low-frequency limit. The PES given by expression (1) was chosen so that the coordinates X and $\{Y_k\}$ coincide with the normal coordinates of the transition state. Since changes in the geometry are determined only by the L- and G-coupling constants, the spectral densities can be directly found by comparing the equilibrium geometries of the ground and transition states.

The equilibrium geometries, eigenfrequencies, and energies of the ground and transition states of MA molecule have been the subject of numerous quantum-chemical studies[26—33] aimed at evaluating the accuracy of different computational methods. For instance, it is known that various Hartree—Fock (HF) methods underestimate the contribution of electron correlation. This leads to extension of the proton transport length, which is mainly due to displacement of the proton along the direction perpendicular to the hypothetical line connecting the O atoms (see Fig. 1). As a result, the barrier height appears to be overestimated (7.9—10.3 kcal mol^{-1} according to different authors) as compared to the upper bound determined from the results of ^{1}H NMR studies (6.1 kcal mol^{-1}).[34] The inclusion of electron correlation at the second-order Møller—Plesset level of perturbation theory[28] is more correct and reduces the perpendicular displacements of the proton, thus making the ground state and transition state structurally similar and lowering the barrier.

The distinguishing features of computational methods based on the density functional theory (DFT) are overestimation of the hydrogen-bond energy, shortening of the O—O distance, lengthening of the O—H bond, and a decrease in the barrier height.[35] Calculations by the coupled cluster method at the CCSD(T) level gave more correct estimates of the barrier height, *viz.*, 4.3 [26] and 3.9 [27] kcal mol^{-1}. It has been shown[26,27] that the results of DFT calculations with the B3LYP exchange-correlation functional[36,37] vary only slightly on going from the 6-311G** basis set to the extended 6-311G(2df,2p) basis set and that basis set extension aimed at obtaining better estimates does not furnish the desired result. Barrier heights obtained from DFT calculations (2.8—3.0 kcal mol^{-1}) remain underestimated as compared to those found by the coupled cluster method.

In this work, we compared the parameters of several Hamiltonians found using the results of quantum-chemical calculations carried out by different methods (Tables 1 and 2). The equilibrium ground-state and transition-state geometries of the fragment containing the hydrogen bond were obtained from HF/6-31G**, MP2/6-311G**, MP4SDQ/6-31G**, and DFT (B3LYP/6-311+G(2dp))

Table 1. Geometric parameters of the O—H—O fragment[a] in the ground and transition states of malonaldehyde molecule and the heights of adiabatic potential barrier calculated by different quantum-chemical methods

Parameter	Experiment[1b]	HF/ 6-31G**	MP2/ 6-311G**	MP4SDQ/ 6-31G**	B3LYP/ 6-311+G(2d,p)	VSXC/ cc-pVTZ [27]
Bond			d/Å			
O(1)—H(1)	0.969	0.956/1.188	0.991/1.198	0.981/1.201	1.002/1.209	0.992/1.215
O(2)—H(1)	1.68	1.881/1.188	1.682/1.198	1.780/1.201	1.670/1.209	1.723/1.215
O(1)—O(2)	2.574	2.681/2.323	2.585/2.358	2.645/2.356	2.570/2.369	2.607/2.381
Angle			ω/deg			
C(1)—O(1)—H(1)	106.3	109.40/102.78	104.70/100.56	106.41/101.51	106.07/101.89	106.24/101.53
C(2)—C(1)—O(1)	124.5	126.40/121.98	124.40/121.89	125.20/121.91	123.88/121.65	124.31/121.76
Barrier			V_{ad}/kcal mol^{-1}			
	≤6.1	10.34	3.45	5.96	2.86	3.70

[a] Ground-state/transition-state parameters.
[b] Ground-state parameters.

Table 2. Selected parameters of the PES of proton transfer in MA molecule calculated by different quantum-chemical methods

Computational method	V_{ad} /kcal mol^{-1}	Ω_0 /cm^{-1}	V_{ad}/V_{1D}	ρ_G	$\tilde{\rho}_G$	ρ_L	$\tilde{\rho}_L$	Δ /cm^{-1}	γ
B3LYP/6-311+G(2d,p)[a]	2.86	3127	3.912	0.738	0.317	0.039	0.018	123.2	5.81
MP2/6-311G**[a]	3.45	3147	3.894	0.743	0.319	0.043	0.019	66.7	6.49
MP4SDQ/6-31G**[a]	5.96	3241	3.705	0.730	0.317	0.032	0.014	5.06	9.56
HF/6-31G**[a]	10.34	3380	3.689	0.729	0.311	0.024	0.012	0.05	14.46
VSXC/cc-pVTZ [27]	3.70	3155[b]	3.855[b]	0.739[b]	0.316[b]	0.038[b]	0.017[b]	51.2[b]	6.80[b]
Optimized PES[a]	4.30	3025	3.79	0.741	0.317	0.034	0.015	21.6	7.74

[a] This work.
[b] For the equilibrium ground-state and transition-state geometries calculated[27] assuming that the eigenfrequencies and eigenvectors are the same as those obtained by the MP4SDQ/6-31G** method.

calculations and in agreement with the above-mentioned characteristic features of corresponding computational methods.

As the barrier height decreases, the differences between the calculated and experimental frequencies of normal vibrations also decrease. Nevertheless, they remain as large as ~200 cm^{-1} for the high-frequency active vibrations even in the case of B3LYP/6-311+G(2dp) calculations (Table 3). On the other hand, the dimensionless transverse frequencies are less sensitive to the computational method and vary by less than 5% as the barrier height changes from 2.8 to 6.0 kcal mol^{-1}. Moreover, calculations using the above-mentioned methods give nearly the same results for both the ground-state and transition-state eigenvectors of normal vibrations.

An analogous picture is observed for the main parameters of the dimensionless PES as well as the spectral densities and dimensionless frequencies in spite of substantial variations of the calculated barrier heights (from 2.8 to 10.3 kcal mol^{-1}) and corresponding tunneling splittings (by more than three orders of magnitude). This means that different PES reconstructed using the results of quantum-chemical calculations by the above-mentioned methods can be matched by scaling only one parameter, *viz.*, the quasiclassical parameter γ. Scaling invariance allows optimization of the Hamiltonian in such a way that the calculated ground-state tunneling splitting coincides with the experimental value.

Tunneling splitting in the vibrational ground state is calculated using the following formula[3,4,11]

$$\Delta_0 = \hbar\Omega_0\sqrt{\gamma}\, B_{\{0k\}}\exp(-\gamma W^*), \qquad (7)$$

where the prefactor $B_{\{0k\}}$ is independent of γ and the action W^* between the potential minima depends on the modified spectral densities (6) and the shape of the 1D potential. If both these parameters are constants, $\ln\Delta_0$ is a linear function of the quasiclassical parameter γ. The spectral densities $\tilde{\rho}_L$ and $\tilde{\rho}_G$ calculated by different methods have close values (see Table 2). Our MP4 calculations also confirmed that the shape of the 1D potential is "insensitive" to computational methods employed. The optimized value of the quasiclassical parameter (γ_0 = 7.74) was found using the theoretical dependence of $\ln\Delta_0$ on γ and the experimental tunneling splitting (Fig. 2). The adiabatic barrier height (4.30 kcal mol^{-1}) corresponding to this γ_0 value was determined using the linear dependence of V_{ad} on γ. The dimensionless frequencies, interpolated between the MP2 and MP4 data, were calculated using the γ_0 value and then scaled by a factor of 0.95.[39] We found that the

Table 3. Frequencies of normal vibrations (cm^{-1}) in the ground (ν_0) and transition ($\nu_\#$) states of MA molecule

Normal ground-state//transition-state modes		ν_0, experiment[38]	$\nu_0//\nu_\#$				
			HF	MP2	MP4	B3LYP	Scaling*
$\delta(OH)/\delta(CH_4)//\delta(OH)/\nu(OH)$	(ν_8)	1379	1497//1780i	1440//1258i	1454//1493i	1389//1164i	1374//1290i
Ring deformation// Ring deformation	(ν_2)	510	530//614	513//580	507//578	524//579	485//550
$\delta(CH)//\delta(CH_3)$	(ν_5)	1092	1211//1201	1115//1112	1136//1140	1118//1115	1068//1068
$\delta(CH)/\nu(C{=}O)//\delta(CH)$	(ν_7)	1339	1535//1427	1421//1358	1444//1363	1405//1331	1359//1292
$\delta(CH_3)/\nu(CC)//\delta(CH_3)/\nu(CC)$	(ν_9)	1444	1600//1629	1483//1516	1510//1541	1481//1507	1420//1450
$\nu(C{=}O)/\delta(OH)//\nu(C{=}O)/\delta(OH)$	(ν_{10})	1588	1770//1717	1667//1709	1694//1683	1627//1612	1595//1613
$\nu(CH_2)//\nu(CH)$	(ν_{12})	2848	3178//3294	3028//3138	3071//3187	2970//3084	2894//3001
Ring deformation// Ring deformation	(ν_1)	282	271//682	267//635	272//637	277//620	256//604
Ring deformation// Ring deformation	(ν_3)	873	957//1030	896//953	899//959	896//950	852//908
$\nu(C{-}C)//\nu(C{-}C)$	(ν_4)	980	1035//1140	1006//1078	1003//1096	1002//1059	954//1031
$\delta(CH_2)/\nu(C{-}O)//\delta(CH_2)/\nu(C{-}O)$	(ν_6)	1255	1378//1499	1299//1393	1305//1406	1287//1370	1236//1329
$\nu(C{=}O)/\nu(C{=}C)//\nu(C{=}O)/\nu(C{=}C)$	(ν_{11})	1652	1928//1812	1718//1674	1766//1699	1691//1633	1652//1600
$\nu(OH)//\nu(OH)/\delta(OH)$	(ν_{15})	2960	3938//2053	3312//1908	3547//1940	3214//1897	3242//1826
$\nu(CH)//\nu(CH)$	(ν_{13})	2855	3369//3293	3211//3137	3266//3187	3107//3084	3073//3000
$\nu(CH_3)//\nu(CH_3)$	(ν_{14})	2865	3395//3421	3272//3290	3306//3331	3174//3230	3122//3142
$\tau(C{=}C)//\tau(C{=}C)$	(ν_{17})	384	424//420	376//354	378//362	399//395	358//340
$\gamma(CH_3)//\gamma(CH)$	(ν_{18})	768	857//823	777//771	779//768	784//779	740//731
$\gamma(CH)//\gamma(CH)$	(ν_{20})	966	1131//1135	1004//968	992//984	1043//993	949//926
$\gamma(OH)//\gamma(OH)$	(ν_{19})	878	829//1429	897//1326	856//1334	1019//1311	836//1263
$\tau(C{-}C)//\tau(C{-}C)$	(ν_{16})	252	248//391	273//377	258//379	288//370	253//359
$\gamma(CH)//\gamma(CH)$	(ν_{21})	1028	1169//1189	1045//1046	1055//1069	937//1043	997//1003

* The frequencies were determined by interpolation of the results obtained at the MP2 and MP4 levels of theory with $\gamma = 7.74$ and a scale factor of 0.95.

results of dynamics calculations vary only slightly after replacement of the calculated frequencies by the experimental ground-state values.

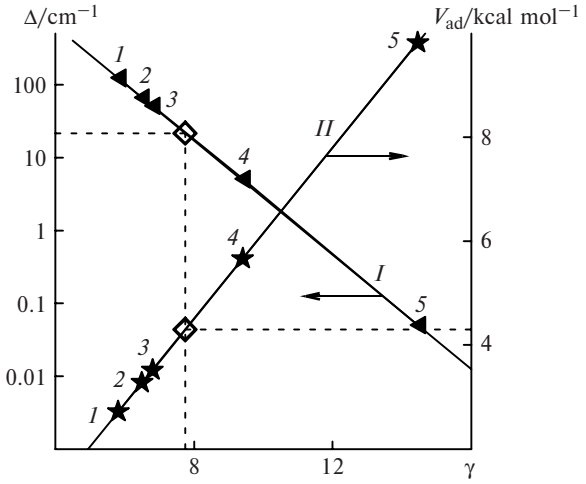

Fig. 2. Dependences of vibrational ground-state tunneling splitting (*I*) and height of adiabatic potential barrier (*II*) on the quasiclassical parameter γ obtained using the results of quantum-chemical calculations by the B3LYP/6-311+G(2d,p) (*1*), MP2/6-311G** (*2*), VSXC/cc-pVTZ (*3*), MP4SDQ/6-31G** (*4*), and HF/6-31G** (*5*) methods. Position of the experimental tunneling splitting corresponding to $V_{ad} = 4.30$ kcal mol^{-1} and $\gamma_0 = 7.74$ is shown by a square.

The characteristic frequency Ω_0 was determined from the relationship

$$V_{ad}/(\hbar\Omega_0) = 0.25\gamma_0(1 - \rho_G), \quad (8)$$

which follows from Eqs. (1) and (5) provided that the 1D barrier and the spectral densities retain their shapes on scaling. Selected parameters of the optimized PES are listed in Table 2 (a detailed description of the Hamiltonian can be obtained upon request *via* e-mail).

We will now outline the salient features of the reconstructed Hamiltonian. The major contribution to the 1D potential given by expression (2) comes from the term with $m = 2$. The V_3/V_2 and V_4/V_2 ratios are small (-0.067 and 0.046, respectively). The rectilinear generalized tunneling coordinate does not correspond to the linear path in Cartesian coordinates (Fig. 3). The 1D path is curvilinear since the ν_8 vibration initially directed along the X coordinate in the transition state is coupled with transverse vibrations in the case of large-amplitude deviations. Due to strong G-couplings, the 1D barrier (~16.97 kcal mol^{-1}) is nearly four times higher than the adiabatic barrier. This is a quantitative characteristic of vibrationally assisted tunneling.

The main properties of the L-, G-, and Sq-coupling constants are as follows. First, linear couplings are so weak that the Sq-couplings are predominant for all L-vibrations. Second, the effect of G-coupling is partly

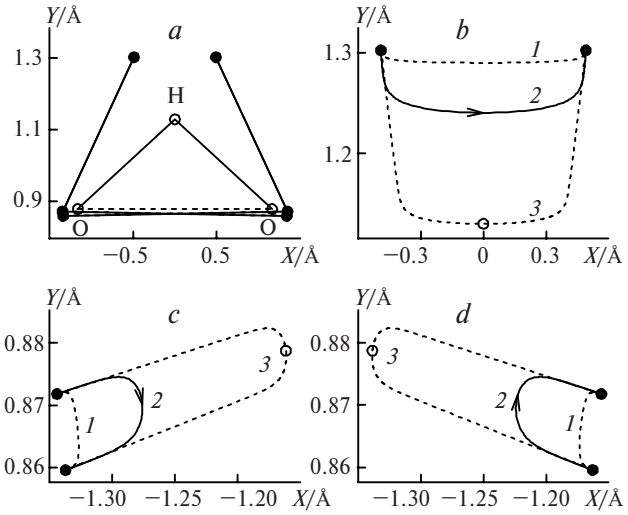

Fig. 3. Deformation of the fragment containing the hydrogen bond (*a*) and displacements of the H (*b*) and O atoms (*c*, *d*) calculated using the optimized Hamiltonian: 1D path (*1*), MEP (*2*), and ETT (*3*). Displacements of O atoms are shown enlarged. All the plots were constructed in Cartesian coordinates.

compensated for by strong negative Sq-coupling with the low-frequency vibration ν_1. Third, G-coupling and positive Sq-coupling with the vibration ν_{15} make the largest promoting contribution to the tunneling splitting. Fourth, resonance effect is observed for the vibrations ν_{13} and ν_{14}. Finally, all low-frequency Sq-vibrations are inactive. It has been shown[6] that the *X*-dependent diagonal elements of the kinematic matrix (the effective masses of all motions) change the transverse frequencies along the tunneling path similarly to the Sq-couplings, whereas the off-diagonal matrix elements affect the tunneling path curvature in Cartesian coordinates (see Fig. 3). Both active G-vibrations, ν_1 and ν_{15}, are characterized by strong kinematic coupling with the *X* coordinate and with each other.

A salient feature of the multidimensional PES of MA molecule is mixing of the ground-state normal modes in the more symmetrical transition state.[21] Among the *YY′*-interactions, two pairs of L-vibrations (ν_7, ν_9 and ν_{10}, ν_{12}) and three G-vibrations (ν_6, ν_{12}, and ν_{15}) are strongly coupled. However, they have little effect on the tunneling dynamics due to the weak coupling with the tunneling coordinate. On the contrary, coupling of G-vibrations ν_1 and ν_6 with the ν_8, ν_{15} as well as ν_4, ν_{15} vibrations, respectively, affects the tunneling splitting magnitude.

Tunneling dynamics

Rapid convergence of perturbative expansion over the coupling constants is achieved if the spectral density is less than 0.5.[3,4] High spectral density of G-vibrations for the MA molecule ($\rho_G = 0.73$) means that the perturbative solutions of the equations of motion and the quasiclassical equations converge too slowly and higher-order terms of the expansion should be taken into account. Additionally, strong potential and kinematic *YY′*-couplings are responsible not only for mixing of transverse modes, but also for the appearance of *X*-dependent anharmonicity affecting the ETT shape and the action. Higher-order solutions include both the effects. In particular, such solutions of the Hamilton—Jacobi (HJE) quasiclassical equations[4] and the transport equation have been considered in studies of tunneling dynamic in hydrogen peroxide molecule.[8,12]

The *n*th order action along the ETT can be expanded in powers of transverse coordinates with *X*-dependent coefficients:

$$W(X,\{Y_k\}) = W_0(X,\{Y_k\}) + \sum_k \left(\delta W_k^{(2)}(X) + \delta W_k^{(4)}(X) + \ldots\right) + \sum_k \left(F_k^{(1)}(X) + F_k^{(2)}(X) + \ldots\right) Y_k + \sum_{kk'} \left(F_{kk'}^{(1)}(X) + F_{kk'}^{(2)}(X) + \ldots\right) Y_k Y_{k'} + \sum_{k,k',k''} \left(F_{kk'k''}^{(1)}(X) + F_{kk'k''}^{(2)}(X) + \ldots\right) Y_k Y_{k'} Y_{k''} + \ldots \quad (9)$$

Here, the superscript denotes the order of the HJE and $W_0(X,\{Y_k\})$ is the action in the system of separable trial functions, which fulfills the zero-order HJE (the case of zero coupling constants):

$$\partial W_0^{L(R)}/\partial X = (2V_0(X))^{1/2}, \quad \partial W_0^{L(R)}/\partial Y_k = \pm\omega_k Y_k. \quad (10)$$

Two branches of solutions of the first equation in (10) correspond to the exponents (actions) of the localized wavefunctions of the left (L) and right (R) potential wells.[4] The second equation in (10) and the second term in expression (9) describe the contributions of the *X*-independent transverse coordinates. It should be noted that only the even-order terms contribute to the action between the potential minima.

Both potential and kinematic L- and G-couplings contribute to all the terms beginning with $n = 2$, whereas the Sq- and *YY′*-couplings make contributions to the terms with $n \geq 4$. The third term in Eq. (9) defines the ETT as the minimum action curve and the fourth and fifth terms describe the *X*-dependent coupling of transverse vibrations and their anharmonicity, respectively. The functions $F_k^{(N)}(X)$, $F_{kk'}^{(N)}(X)$, ... are found from perturbative solution of the HJE in the first, second, ..., *n*th order with respect to the coupling constants. Recently,[8,12] it has been shown that consideration of *X*-independent anharmonicity is significant only for the active transverse vibrations. Much stronger is the effect of *XY*- and *YY′*-couplings responsible for cross-anharmonicity of transverse vibrations and thus for changes in the ETT shape. The fourth-order actions W^L and W^R were calculated using analytical expressions for the functions $F_k^{(N)}(X)$ and $F_{kk'}^{(N)}(X)$.[8] These

two actions determine the exponents of the quasiclassical wavefunctions of the localized states $\Psi_{n\{nk\}}^{L(R)}$.

Expansions of the ETT and action in powers of coupling constants (9) are monotonic. Since the major contribution to the action comes from G-couplings, the action decreases monotonically as the perturbation theory order increases. Hence the barrier height corresponding to the *n*th-order tunneling splitting can be considered as the lower bound of the exact action value. To find the upper bound of the action, one can construct the second perturbative solution for which the MEP and corresponding adiabatic potential will serve as zero approximation. This perturbative expansion also monotonically converges to the exact action value.

Thus, the true tunneling path passes in the region between two perturbative solutions of the equations of motion (ETT-I and ETT-II). The actions on these extreme tunneling trajectories determine the confidence intervals for the parameters of the quasiclassical wavefunctions. The contributions of different vibrations to the action on the ETT-I and ETT-II are listed in Table 4. Narrowness of the confidence intervals is illustrated by small differences between the contributions to the action on the ETT-I and ETT-II (see columns 2 and 3 in Table 4) and characterizes the accuracy of the PIA. The second-order solution along the ETT-II corresponds to $\gamma_0 = 7.84$ and $V_{ad} = 4.39$ kcal mol^{-1}. By comparing the two perturbative solutions we get 4.34±0.4 kcal mol^{-1} for the adiabatic barrier height in the MA molecule.

Tunneling splittings are described by the generalized Lifshitz—Herring formula[4]:

$$\Delta_{n\{n_k\}} = \frac{\hbar\Omega_0}{\gamma} \int \Psi^{L}_{n\{n_k\}} \nabla \Psi^{R}_{n\{n_k\}} \Big|_{X=0} d\{Y_k\} = \\ = \frac{\hbar\Omega_0}{\gamma} \left(\Delta^{(0)}_{n\{n_k\}} + \sum_{n'\{n'_k\}} a_{n\{n_k\}n'\{n'_k\}} \Delta^{(0)}_{n'\{n'_k\}} \right), \quad (11)$$

where integration is performed over the dividing surface and $\Delta^{(0)}{}_{n\{n_k\}}$ are the tunneling splittings of the "pure" states with constant values of vibrational quantum numbers $\{n,n_k\}$. Analogously to the reaction path Hamiltonian formalism, these splittings can be represented as products of the transition probability along the reaction path and the transverse prefactor:

$$\Delta^{(0)}_{n\{n_k\}} = B_{\{n_k\}} \bar{\Delta}^{(0)}_{n\{n_k\}}, \qquad B_{\{n_k\}} = \prod_k \left(\frac{\omega_k^{\#}}{\omega_k^{\min}} \right)^{n_k+0.5}, \quad (12)$$

where $\bar{\Delta}^{(0)}{}_{n\{n_k\}}$ corresponds to the action along the ETT and the prefactor characterizes changes in the transverse frequencies upon the transition (the prefactor magnitude is determined by the transition-state/ground-state frequency ratio). Due to *XY*-couplings, vibrational quantum numbers are not conserved and the quasiclassical

Table 4. Contributions of particular transverse vibrations to the action and ground-state tunneling splitting of MA molecule

Vibration		δW^*, $n = 4$ (ETT-I)	δW^*, $n = 2$ (ETT-II)	δW^*, $n = 4$ (ETT-I), potential and kinematic couplings	$\exp(-\gamma\delta W^*)$, $n = 4$, ETT-I	Sq-Factor, $B_{\{0k\}}$ ★
		Potential couplings				
ν_2	(L)	0.0008	0.0009	0.0001	0.999	0.962
ν_5	(L)	0.0011	0.0013	0.0004	0.997	1.164
ν_7	(L)	0.0014	0.0015	0.0026	0.980	1.134
ν_9	(L)	0.0027	0.0030	0.0012	0.991	0.918
ν_{10}	(L)	0.0091	0.0102	0.0045	0.966	0.887
ν_{12}	(L)	0.0	0.0	0.0	1.0	0.918
ν_1	(G)	−0.1254	−0.1272	−0.1541	3.296	0.891
ν_3	(G)	−0.0165	−0.0192	−0.0226	1.191	0.926
ν_4	(G)	−0.0154	−0.0175	−0.0122	1.099	1.025
ν_6	(G)	−0.0201	−0.0222	−0.0261	1.223	1.115
ν_{11}	(G)	−0.0019	−0.0022	−0.0026	1.020	1.081
ν_{15}	(G)	−0.1092	−0.1131	−0.0983	2.140	1.332
ν_{13}	(G)	−0.0173	−0.0185	−0.0179	1.149	0.963
ν_{14}	(G)	−0.0111	−0.0117	−0.0108	1.087	0.986
ν_{17}	(Sq)	—	—	—	—	1.012
ν_{18}	(Sq)	—	—	—	—	1.010
ν_{20}	(Sq)	—	—	—	—	0.960
ν_{19}	(Sq)	—	—	—	—	0.931
ν_{16}	(Sq)	—	—	—	—	0.980
ν_{21}	(Sq)	—	—	—	—	0.991

★ Calculated using formula (7).

wavefunctions are linear combinations of the wavefunctions of the "pure" states. The coefficients $a_{n\{n_k\}n'\{n'_k\}}$ can be found from expansion of the solutions of the transport equation over the basis set of the "pure" states.[4,8]

The contribution of each transverse vibration to the action can be considered as the sum of kinematic L(G)-components and Sq-components (see Table 4). Since all L-coupling constants are small, the effect of Sq-couplings is predominant for the L-vibrations. Particular factors in expression (12) can substantially differ from unity due to the Sq-couplings. Nevertheless, Sq-vibrations have little effect on the splitting ($B\{n_k\}$ = 0.884) since Sq-couplings of opposite sign partly cancel one another. The largest increase in the tunneling splitting is due to the promoting effect of the ν_1 and ν_{15} vibrations, which increase the 1D splitting in the ground state by a factor of 8.4. For comparison, the total effect of all other vibrations (except for the ν_1 and ν_{15} vibrations) leads to an increase in the ground-state tunneling splitting by a factor of 1.74. The contributions of G- and Sq-couplings of the inactive G-vibrations are comparable.

By and large, proton transfer in the MA molecule can be described as follows. Motion along the tunneling coordinate directed along the ν_8 vibration in the transition state leads to lengthening of the O—H bond and to a decrease in the C—O—H angle (see Fig. 3). The effect of two promoting vibrations, ν_1 and ν_{15}, results in the low-frequency ring deformation and high-frequency symmetric deformation of the hydrogen bond, which reduces both the tunneling path and the barrier along the ETT. These three transition-state normal modes are strongly mixed with other modes of the same symmetry along the tunneling path, so that most of the ground-state A′-type modes appear to be involved in the tunneling transition. From this point of view, active modes cannot be selected from the spectrum of weakly coupled modes. Coupling also causes substantial changes in the transverse frequencies along the ETT (Fig. 4). Being much larger than the X-independent ground-state anharmonicity, the anharmonicity due to tunneling transitions has little effect on the tunneling splittings.

Since the frequency of the promoting G-vibration ν_{15} is close to Ω_0 (see Tables 2 and 3), tunneling corresponds to neither the adiabatic limit ($\omega\to\infty$) nor the low-frequency limit ($\omega\to0$) and the ETT deviates from both the MEP and the 1D path. The shape of the ETT and MEP in the (X, Y_1, Y_{15}) configuration space is shown in Fig. 5. According to the generalized Fukui theorem,[3,16] the ETT starts along the direction of the lowest-frequency vibration, ν_1, and then deviates along the directions of the ν_8 and ν_{15} vibrations. The ETT intersects the dividing surface at a point between the saddle point and the point Y_k = 0. The barrier height along the ETT is intermediate between those of the adiabatic and 1D barriers (8.09 *vs.* 4.34 and 16.18 kcal mol^{-1}, respectively).

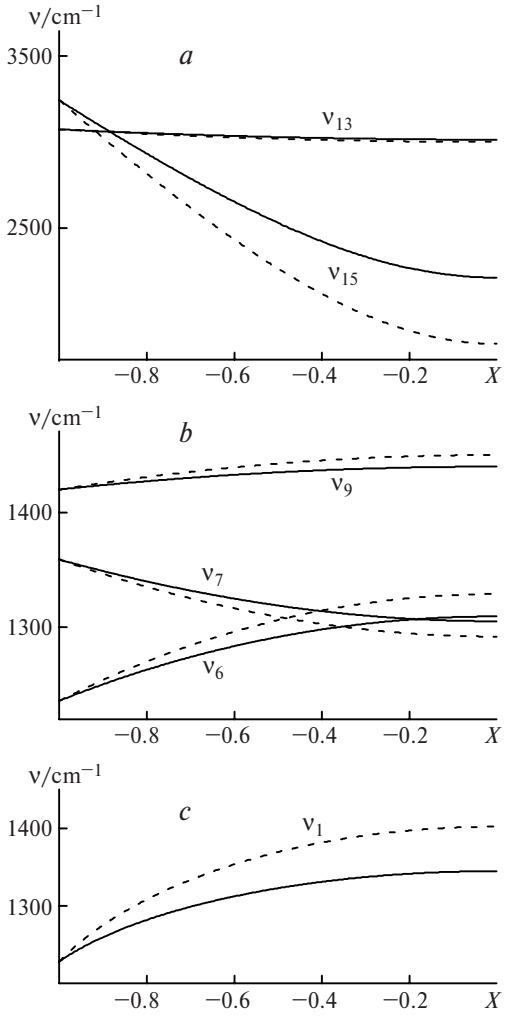

Fig. 4. Changes in the ν_{13}, ν_{15} (*a*); ν_6, ν_7, and ν_9 (*b*); and ν_1 (*c*) transverse frequencies of active vibrations along the MEP (dashed lines) and ETT (solid lines) calculated using the optimized Hamiltonian.

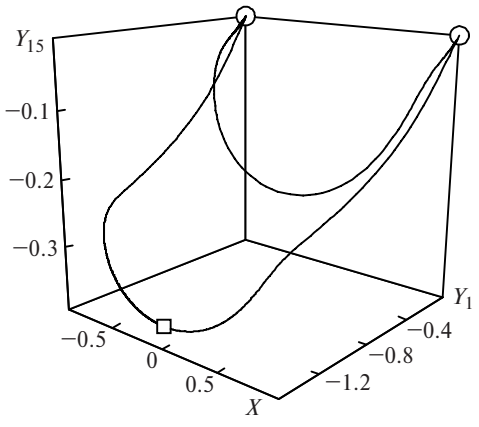

Fig. 5. The shape of the ETT and MEP in the three-dimensional configuration space of dimensionless coordinates X, Y_1, and Y_{15}. Transverse displacements are shown enlarged.

The barrier along the ETT is lower than the 1D barrier. Its height is determined by the modified spectral density (6), whereas the adiabatic and 1D barriers are related by formula (5), which depends on the spectral density (4). The modified spectral density for proton transfer in the MA molecule is nearly half as large as in the adiabatic limit (see Table 2), so that the action along the ETT is larger than along the MEP. Transverse vibrations assist the ground-state tunneling splitting in the 1D potential (0.87 cm^{-1}) and increase it by a factor of 25. In the adiabatic limit, this splitting should be 2.6 times larger (55.73 cm^{-1}).

To calculate tunneling splittings in the vibrational excited states using relationships (11) and (12), the $\Delta^{(0)}{}_{n\{n_k\}}$ and mixing coefficients $a_{n\{n_k\}n'\{n'_k\}}$ should be known. Since the exponent of the instanton wavefunctions is independent of the quantum numbers, tunneling splittings in the excited "pure" states are due to changes in the transverse mode prefactors (12) caused by the effect of Sq-couplings. Tunneling splittings increase (decrease) if the average transverse frequency along the ETT is higher (lower) than that at the PES minimum. Mixing of the "pure" states with different vibrational quantum numbers is determined by the *XY*- and *YY′*-couplings. Mixing of the $(0, 1_k)$ states with small tunneling splittings and the $(1, 0_k)$ state with large splitting always increases tunneling splittings in the mixed excited states of the G- and L-vibrations. *YY′*-Couplings reduce corrections to the tunneling splittings of vibrational levels for strongly coupled vibrations and increase analogous corrections in the case of inactive vibrations.

The magnitudes of tunneling splittings of all vibrational excited levels in the MA molecule (the first excited levels are considered!) are listed in Table 5. For the ν_8 vibration, the splitting of the first excited level is nearly an order of magnitude larger than the ground-state splitting since the former level is near the barrier top. The splitting of the first excited vibrational level in the 1D potential (615 cm^{-1}) was determined by diagnalization of the 1D Hamiltonian matrix. In the case of multidimensional PES it decreases to 503 cm^{-1} due to the coupling with transverse vibrations. L-Vibrations ν_2, ν_5, ν_{10}, and ν_{12} are weakly coupled and the tunneling splitting changes due to the Sq-coupling. *YY′*-Coupling of the L-vibration ν_9 with the G-vibration ν_6 determines an increase in the corresponding splitting despite the negative Sq-coupling constant. The coupling between the ν_6 and ν_7 vibrations assists the splitting in the $(0, 1_7)$ state.

The effect of *XY*-coupling dominates in the case of the G-vibration ν_1. Due to this coupling, the $(0, 1_1)$ level is strongly mixed with the $(1, 0_1)$ level despite the large energy difference between these states. The resulting slight increase in the tunneling splitting of the $(0, 1_1)$ level is due to mutual cancellation of large contributions of opposite sign, namely, the positive contribution of the G-coupling and the negative contribution of the Sq-coupling. The increase in the splitting of the G-vibration ν_3 is due to *XY*- and *YY′*-couplings with the vibration ν_1. *YY′*-Coupling between the vibrations ν_4 and ν_6 promotes tunneling in the $(0, 1_4)$ state. Large splitting of the levels $(0, 1_6)$ and $(0, 1_{15})$ is due to combination of relatively strong *XY*-couplings and positive Sq-couplings.

Table 5. Tunneling splittings (cm^{-1}) in vibrational spectra of MA, MA-d_1, MA-d_4, and MA-^{13}C

State	ETT-I				ETT-II, MA
	MA	MA-d_1	MA-d_4	MA-^{13}C	
0	21.6	3.0	2.84	20.60	21.6
$1\nu_8$	503.19	346.14	202.36	544.53	532.12
$1\nu_2$	19.75	2.47	3.46	18.53	19.71
$1\nu_5$	25.57	4.27	4.50	23.77	25.63
$1\nu_7$	27.23	3.77	3.74	25.87	27.91
$1\nu_9$	23.70	3.06	4.00	22.40	23.72
$1\nu_{10}$	17.27	4.29	3.79	16.31	16.91
$1\nu_{12}$	20.77	2.70	3.18	19.62	20.75
$1\nu_1$	33.75	6.52	5.79	30.05	37.12
$1\nu_3$	26.52	4.00	4.17	26.76	28.71
$1\nu_4$	29.71	4.28	3.19	29.51	31.78
$1\nu_6$	38.11	6.68	3.93	34.24	40.93
$1\nu_{11}$	22.20	3.20	6.18	20.97	22.40
$1\nu_{15}$	64.02	7.10	8.15	55.92	71.70
$1\nu_{13}$	163.18	6.74	73.12	146.22	174.30
$1\nu_{14}$	127.12	5.30	60.43	118.03	132.20
$1\nu_{17}$	22.70	3.18	3.53	21.39	22.73
$1\nu_{18}$	22.47	3.15	2.91	21.19	22.45
$1\nu_{20}$	18.56	2.11	2.09	17.54	18.12
$1\nu_{19}$	15.82	3.10	1.81	14.18	14.89
$1\nu_{16}$	18.03	2.52	2.47	17.50	17.91
$1\nu_{21}$	20.63	2.87	3.03	19.45	20.52

A salient feature of the MA molecule is resonance between the antisymmetrical deformation stretching OH vibration ν_8 and its symmetrical analog, ν_{15}. Two new resonances appear between the ν_8 vibration and the stretching CH vibrations ν_{13} and ν_{14} whose frequencies are close to the doubled frequency of ν_8. In the case of H/D substitution in the OHO fragment (we will denote this isotopomer MA-d_1), the ν_8—ν_8 resonance occurs, whereas the other two resonances disappear. All the three resonances are predicted for the perdeuterated MA (MA-d_4). It has been mentioned[7,10,11] that vibrational mode selectivity of tunneling transitions provides the possibility for chemical processes with large heavy-atom isotope effects to occur. This is also confirmed by the results obtained for the MA-^{13}C isotopomer. Changes in the tunneling splittings of excited vibrational states upon $^{13}C/^{12}C$ substitution are much larger than changes in the vibrational frequencies. The accuracy of the PES reconstruction carried out in this work allows only prediction of the ν_8—ν_{13} and ν_8—ν_{13} resonances. Quantitative calculations of the splittings of the resonance levels requires more reliable frequencies.

* * *

The results of the multidimensional tunneling dynamics study of MA molecule reported in this work are qualitatively consistent with those obtained in previous studies. The key role of the G-vibrations ν_1 and ν_{15} in the vibrationally assisted proton transfer in MA molecule has been reported earlier.[3,21] However, the effect of these vibrations was strongly overestimated to provide the desired penetrability of the too high potential barrier used previously[21] (10.3 and 39.3 kcal mol^{-1} for the adiabatic and 1D barriers, respectively) and to reproduce the experimental splitting value.

Calculations with model 2D Hamiltonians[17,38, 40—42] correctly reproduce the barrier height (4.98 and 18.01 kcal mol^{-1} for the adiabatic and 1D barriers, respectively). In this simplified model, the frequency of the effective transverse vibration ($\omega = 0.71$) used for the simulation of the whole manifold of transverse vibrations is chosen to be intermediate between the ν_1 and ν_{15} frequencies to provide a correlation between the 2D ETT and the real deviation of the ETT from the MEP. In spite of qualitative similarity with the results of earlier studies, multidimensional tunneling dynamics considered in this work is much more complicated than that described previously. Resonances and X-dependent YY'-interactions lead to much stronger coupling between normal vibrations in the excited states compared to the ground state. Weakly coupled transverse vibrations are also involved in tunneling dynamics, so that the approximation of normal vibrations with conservation of quantum numbers is no longer valid for the MA and related nonrigid molecules characterized by sufficiently large number of degrees of freedom. Usually, the number of degrees of freedom explicitly taken into account is reduced to simplify the problem; however, this violates the resonance conditions and leads to inevitable distortions of transition dynamics.

Similarly to the dynamics of hindered rotation in hydrogen peroxide molecule,[8] the PIA allows a satisfactory solution of the multidimensional dynamics problem for the MA molecule. Reliability of our results is limited by the accuracy of the PES reconstruction rather than tunneling dynamics analysis based on the results of these calculations. Of course, scaling invariance allows optimization of parameters of the Hamiltonian using the experimental vibrational frequencies and ground-state tunneling splittings. On the other hand, the vibration-tunneling spectra calculated in this work should be verified experimentally. This would provide the possibility of (i) solving the inverse dynamics problem, *viz.*, reconstruction of the Hamiltonian, for a nonrigid molecule and (ii) determining the accuracy of different high-level quantum-chemical methods under actual experimental conditions. Two main salient features of proton transfer in MA molecule, namely, occurrence of resonances and tunneling-induced cross-anharmonicity of transverse vibrations, are independent of possible refinement of parameters of the Hamiltonian.

This work was financially supported by the Russian Foundation for Basic Research (Project No. 00-03-32938a).

References

1. S. L. Baughcum, R. W. Duerst, W. F. Rowe, Z. Smith, and E. B. Wilson, *J. Am. Chem. Soc.*, 1981, **103**, 6296.
2. T. Baba, T. Tanaka, I. Morino, K. M. T. Yamada, and K. Tanaka, *J. Chem. Phys.*, 1999, **110**, 4131.
3. V. A. Benderskii, E. V. Vetoshkin, S. Yu. Grebenshchikov, L. von Laue, and H.-P. Trommsdorff, *Chem. Phys.*, 1997, **219**, 119.
4. V. A. Benderskii, E. V. Vetoshkin, L. von Laue, and H.-P. Trommsdorff, *Chem. Phys.*, 1997, **219**, 143.
5. V. A. Benderskii, E. V. Vetoshkin, and H.-P. Trommsdorff, *Chem. Phys.*, 1998, **234**, 153.
6. V. A. Benderskii and E. V. Vetoshkin, *Chem. Phys.*, 1998, **234**, 173.
7. V. A. Benderskii, E. V. Vetoshkin, and H.-P. Trommsdorff, *Chem. Phys.*, 1999, **244**, 273.
8. V. A. Benderskii, E. V. Vetoshkin, and H.-P. Trommsdorff, *Chem. Phys.*, 2000, **262**, 369.
9. V. A. Benderskii, E. V. Vetoshkin, and H.-P. Trommsdorff, *Chem. Phys.*, 2000, **262**, 393.
10. V. A. Benderskii, E. V. Vetoshkin, and H.-P. Trommsdorf, *Izv. Akad. Nauk, Ser. Khim.*, 1999, 2052 [*Russ. Chem. Bull.,* 1999, **48**, 2029 (Engl. Transl.)].
11. V. A. Benderskii, *Izv. Akad. Nauk, Ser. Khim.*, 1999, 2215 [*Russ. Chem. Bull.,* 1999, **48**, 2187 (Engl. Transl.)].
12. V. A. Benderskii, E. V. Vetoshkin, and H.-P. Trommsdorf, *Izv. Akad. Nauk, Ser. Khim.*, 2001, 350 [*Russ. Chem. Bull., Int. Ed.*, 2001, **50**, 366].
13. A. M. Polyakov, *Nucl. Phys.*, 1977, **120**, 429.
14. S. Coleman, *Aspects of Symmetry*, Cambridge Univ. Press, Cambridge, 1985.
15. V. A. Benderskii, V. I. Goldanskii, and D. E. Makarov, *Phys. Reps.*, 1993, **233**, 195.
16. V. A. Benderskii, D. E. Makarov, and C. A. Wight, *Chemical Dynamics at Low Temperatures*, Wiley Interscience, New York, 1994.
17. V. A. Benderskii, S. Yu. Grebenshchikov, D. E. Makarov, and E. V. Vetoshkin, *Chem. Phys.*, 1994, **185**, 101.
18. V. A. Benderskii, S. Yu. Grebenshchikov, G. V. Milnikov, and E. V. Vetoshkin, *Chem. Phys.*, 1994, **188**, 19.
19. V. A. Benderskii, S. Yu. Grebenshchikov, and G. V. Milnikov, *Chem. Phys.*, 1995, **194**, 281.
20. V. A. Benderskii, S. Yu. Grebenshchikov, G. V. Milnikov, and *Chem. Phys.*, 1995, **198**, 19.
21. Z. Smedarchina, W. Siebrand, and M. Z. Zgierski, *J. Chem. Phys.*, 1995, **103**, 5226.
22. Z. Smedarchina, W. Siebrand, and M. Z. Zgierski, *J. Chem. Phys.*, 1995, **104**, 1203.
23. Z. Smedarchina, A. Fernandez-Ramos, and M. A. Rios, *J. Chem. Phys.*, 1997, **106**, 3856.
24. A. Fernandez-Ramos, Z. Smedarchina, M. Z. Zgierski, and W. Siebrand, *DOTT1. 0, A Computer Program to Calcu-*

late Hydrogen-Tunneling Splittings in Molecular Spectra, National Research Council of Canada, Ottawa, KIA, OR6, 1997.
25. Z. Smedarchina, M. Z. Zgierski, W. Siebrand, and P. M. Kozlowski, *J. Chem. Phys.*, 1998, **109**, 1014.
26. V. Barone and C. Adamo, *J. Chem. Phys.*, 1996, **10**, 11007.
27. S. Sadhukhan, D. Munoz, C. Adamo, and G. E. Scuseria, *Chem. Phys. Lett.*, 1999, **306**, 83.
28. M. J. Frish, A. C. Scheiner, and H. F. Schaefer, *J. Chem. Phys.*, 1985, **82**, 4194.
29. Z. Latajka and S. Scheiner, *J. Phys. Chem.*, 1992, **96**, 9764.
30. S. Scheiner, *J. Mol. Struct. (THEOCHEM)*, 1994, **307**, 65.
31. K. Luth and S. Scheiner, *J. Phys. Chem.*, 1994, **98**, 3582.
32. C. W. Bauschlichter and H. J. Patridge, *J. Chem. Phys.*, 1995, **103**, 1768.
33. S. Sirois, E. I. Proynov, D. T. Nguyen, and D. R. Salahub, *J. Chem. Phys.*, 1997, **107**, 6770.
34. R. S. Brown, A. Tse, T. Nakashima, and R. C. Hadson, *J. Am. Chem. Soc.*, 1979, **101**, 3157.
35. R. V. Stanton and K. M. Merz, *J. Chem. Phys.*, 1994, **101**, 6658.
36. C. Lee, W. Yang, and R. G. Parr, *Phys. Rev., B*, 1988, **37**, 785.
37. A. D. Becke, *J. Chem. Phys.*, 1995, **98**, 5648.
38. E. Bosh, H. Moreno, J. M. Lluch, and J. Bertran, *J. Chem. Phys.*, 1990, **93**, 5685.
39. T. Chiavassa, P. Roubin, L. Pizzala, P. Verlaque, and A. Allouche, *J. Phys. Chem.*, 1992, **96**, 10659.
40. T. Carringtton and W. H. Miller, *J. Chem. Phys.*, 1986, **84**, 4364.
41. N. Shida, P. Barbara, and J. E. Almlöf, *J. Chem. Phys.*, 1989, **91**, 4061.
42. T. D. Sewell, Y. Guo, and D. L. Thompson, *J. Chem. Phys.*, 1995, **103**, 8557.

Received December 29, 2000;
in revised form April 9, 2001